Spontaneous emission in one-dimensional photonic crystals

Adán S. Sánchez and P. Halevi
Instituto Nacional de Astrofísica, Óptica y Electrónica, Apdo. Postal 51, Puebla, Puebla 72000, México
(Received 7 January 2005; published 16 November 2005)

We study the spontaneous emission of an atom embedded in a one-dimensional photonic crystal or superlattice using a classical electrodynamic theory of radiation. The rate of emission is a function of the frequency of the emitted photon, the dipole's position and orientation, as well as the geometric and material parameters of the superlattice. The emission spectrum shows an oscillatory behavior which follows the photonic band structure. For TE modes, there are frequency regions where radiative emission is completely prohibited due to the absence of modes with $k_{\|}<\omega/c$; the radiation is then TM polarized. In addition to the radiative modes, there are always evanescent modes with $k_{\|}>\omega/c$ which are waveguided by the dielectric layers. The evanescent contribution to the spontaneous emission is dominant if a dielectric layer is in the near field region of the dipole. For TM modes, emission rates greatly vary for parallel and perpendicular dipole moments. In a photonic crystal with a high filling fraction of the dielectric and perpendicular dipoles located in the low-index layer, the decay rate can be as much as 76 times the free space value for a single atom and 50 times for a gas of atoms. We also find that the rate of emission presents a strong dependence on the atom's position.

DOI: 10.1103/PhysRevE.72.056609 PACS number(s): 42.70.Qs

I. INTRODUCTION

The environment of an excited atom is known to influence its rate of spontaneous emission (SE) [1]. The effect can be explained in terms of a radiating dipole driven by the reflected field at the dipole's position [2], a classical description, or as emission stimulated by the zero-point fluctuations of the electromagnetic field which has a quantum electrodynamical origin. Both approaches to the interaction between radiation and matter yield the same result if the coupling between the atom and the field is weak [3]. In this regime the atomic transition is irreversible and the rate of SE can be calculated perturbatively using the Fermi's golden rule which states that the rate of SE is proportional to the density of optical states. The role of the material surrounding the atom is to alter the density of states (or modal density). If the modal density vanishes, then the SE is prohibited. On the other hand, the rate of SE can also be enhanced over the free space value as a result of a respective increase in the density of states. The decay of an excited atom, the fluorescence of molecules and electron-hole radiative recombination are examples of SE; we will hereafter refer to the atom, molecule, or electron-hole pair simply as emitter or source.

Many experimental and theoretical works considering emitters in environments of varying complexity have been reported. Compared to the decay rate in free space, the rate of SE in an unbounded medium of dielectric constant ϵ is enhanced for $\epsilon>1$ and diminished for $\epsilon<1$ [4]. It has been experimentally [5] and theoretically [6,7] demonstrated that the presence of a metallic interface in the vicinity of fluorescing molecules alters their fluorescence lifetime. Despite its simplicity, the single interface is technologically important and has been the subject of continuous research [8,9]. Recent work on molecular ensembles in this configuration, under various experimental conditions is evidence of current interest [10].

Advancing to the case of an emitter in the presence of two interfaces we can find numerous works. This geometry is important because in semiconductor-based light emitting devices the electron-hole recombination takes place inside a thin layer. On the other hand, two interfaces can also enclose a cavity in its simplest form; this arrangement has been studied using quantum electrodynamical [11–13] and classical [14] approaches. When more than two interfaces are present, the system turns out to be technologically more interesting but also more challenging [15–18]. Among its practical applications we mention optical sensors of molecular fluorescence [19,20], near-field microscopy [21], and light emitting devices [22]. Due to their ability to appreciably alter the density of modes, cavities have been the subject of intense study. They are an essential part of lasers [23]. The studies range from a dipole between two mirrors [24] and Fabry-Perot microcavities [25] to cavities of arbitrary geometry [26,27]. In the last case, it is necessary to resort to numerical methods such as Finite Difference Time Domain. On the other hand, photonic crystals (PCs) are periodic structures that can also drastically alter the density of modes. In fact, if there is periodicity in all three spatial directions and the geometry and materials are judiciously chosen, forbidden frequency bands for light propagation in all directions may appear [28]. A defect in a PC can thus function as a cavity with promising applications [29–31].

Turning to perfect (defectless) PCs, the power emitted by a dipole in infinite one-dimensional (1D) PCs, modeled by a periodic arrangement of Dirac-delta functions ["Dirac comb" superlattice (SL)], was investigated in Refs. [32,33]. The frequency-dependent power emitted into TE modes exhibits slope discontinuities at some on-axis band edges and a notable power enhancement was found when the dipole is located very near to a Dirac function scatterer, presumably due to its coupling to evanescent modes [32]. Because of the absence of evanescent TM-polarized modes in the Dirac comb SL, the calculation of the power emitted into these modes was less successful. The same model of plane scatterers but with a finite number of periods has also been used to study position- and orientation-dependent decay rates [34].

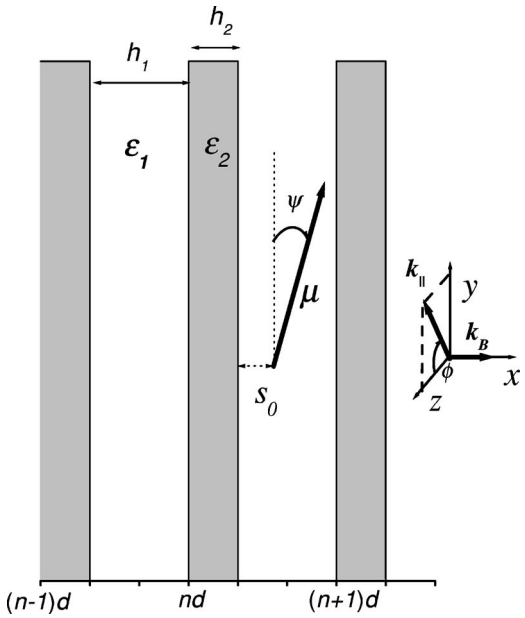

FIG. 1. Atom embedded in a 1D PC. The atom is modeled as a dipole with dipole moment $\boldsymbol{\mu}$ in the xy plane, forming an angle ψ with the y axis. In all figures, $\epsilon_1=1$ and $\epsilon_2=16$, corresponding to Ge. The inset shows the two components of the wave vector, namely the Bloch vector $\mathbf{k}_B$ and the parallel component $\mathbf{k}_\parallel$.

Except in the low-frequency region, the behavior of the SE rate in the inner cells of the finite system and in the infinite crystal results to be similar. As a demonstration of the applicability of their theory of emission in inhomogeneous media, Dowling and Bowden used the Dirac-delta model but they limited the radiation to the direction of the periodicity [35]. Although the same restriction has been used to analyze the rate of emission in 1D PCs made of layers with finite width, a notable band-edge emission enhancement was detected [36].

It must be mentioned that there exist investigations on SE in two- and three-dimensional PCs [37–40]; however, the decay rate of an atom in a perfect and realistically modeled 1D PC remains unexplored. In this paper, the SE rate of an atom embedded in a 1D PC, Fig. 1, is investigated. Here, the emission is allowed in all directions; because the periodic structure possesses mirror symmetry, the solutions of Maxwell's equations decouple into TE- and TM-polarized modes. Glauber and Lewenstein calculated the rate of SE, in the weak-coupling framework, of an atom embedded in an inhomogeneous dielectric medium characterized by an arbitrary position-dependent dielectric constant [4]. In this work, we use the classical formulation, given by Dowling and Bowden [35], of the modal quantum electrodynamical theory of Glauber and Lewenstein. Therefore the transition matrix element is represented by an oscillating dipole with dipole moment $\boldsymbol{\mu}$ whose emitted power P is related to the rate of SE Γ by $\Gamma=P/\hbar\omega$. Moreover, if Γ is normalized by the rate of emission in free space Γ_0, and the corresponding normalization is applied to P, we obtain $\Gamma/\Gamma_0=P/P_0$. Although we do not take into account the local field effect, it would cancel when Γ is normalized by the rate of emission in the corresponding unbounded medium which contains the emitter. The power emitted by a dipole $\boldsymbol{\mu}(=\mu\hat{\boldsymbol{\mu}})$ radiating at frequency ω_0 and located at $\mathbf{r_0}$ can be expressed in terms of the vector potential eigenvectors $\mathbf{a_k}(\mathbf{r_0})$,

$$P_p = \pi^2\omega_0^2\mu^2 \int d^3k |\mathbf{a}_{\mathbf{k}p}(\mathbf{r_0})\cdot\hat{\boldsymbol{\mu}}|^2 \delta(\omega_{\mathbf{k}p}-\omega_0). \quad (1)$$

The index p identifies the two polarization contributions to the total power: $p=$TE and $p=$TM. We should point out that the electric field associated to the potential eigenvector $\mathbf{a_k}(\mathbf{r_0})$ in Eq. (1) is the field in the absence of the emitter and it is different from the field that is actually present in the emitter-1D PC system. Another important physical quantity that only appears implicitly in Eq. (1) is the density of modes: the Dirac-delta function selects the modes that have the frequency of the emitter and therefore contribute to the emitted power. In fact, the expression $d^3k\delta(\omega_{\mathbf{k}p}-\omega_0)$ is the contribution of the element d^3k to the density of modes. Explicit computations of the density of modes for finite 1D PCs using the 1D wave equation [41] and the complete vectorial electromagnetic field [42] have been reported. In order to obtain the power emitted by a dipole embedded in a perfect 1D PC, it is necessary to find the orthonormalized normal modes of the structure, which is done in Sec. II for TE and TM polarized modes. In Sec. III we apply a normalization process to each of these two modes. The normalized modes are used to calculate the emitted power in Sec. IV. The empty-lattice model and the low-frequency limit are investigated in Sec. V. The results are presented and discussed in Sec. VI and the conclusions are given in Sec. VII.

II. NORMAL MODES

In this section, we calculate the normal modes of a SL consisting of alternating layers of materials with dielectric constants ϵ_1 and ϵ_2 and respective thicknesses h_1 and h_2. Each constituent is assumed to be linear, nonmagnetic, and characterized by a real dielectric constant.

A. TE normal modes

The dielectric function $\epsilon(\mathbf{r})$ depends periodically on x and is invariant in the y and z directions $[\epsilon(\mathbf{r})=\epsilon(x)]$; hence for TE polarization, the electric field is given in the Bloch-wave form

$$\mathbf{E_k}(\mathbf{r}) = u_{k_B}(x)e^{ik_Bx}e^{i(k_yy+k_zz)}\hat{\mathbf{e}}_\mathbf{k}, \quad (2)$$

where $u_{k_B}(x)$ is a periodic function with the period d of the SL and $\hat{\mathbf{e}}_\mathbf{k}$ is a unitary vector in the yz plane and perpendicular to $\mathbf{k}_\parallel$ (the wave-vector component parallel to the interfaces which forms an angle ϕ with the z axis, see inset of Fig. 1).

The electric field in each layer of the cell $n=0$ can be written as the combination of two plane waves propagating to the right and left:

$$\mathbf{E}_\mathbf{k}^{(0,j)}(x) = [A_je^{iK_j(x)} + B_je^{-iK_j(x)}]\hat{\mathbf{e}}_\mathbf{k}; \quad (3)$$

$$K_j = \left(\frac{\omega^2}{c^2}\epsilon_j - k_\parallel^2\right)^{1/2}, \tag{4}$$

where

$$j = \begin{cases} 1, & h_2 < x < d, \\ 2, & 0 < x < h_2. \end{cases}$$

The solutions for the nth cell are given by the Bloch theorem:

$$\mathbf{E}_{\mathbf{k}}^{(n,j)}(x) = e^{ink_B d}[A_j e^{iK_j(x-nd)} + B_j e^{-iK_j(x-nd)}]\hat{\mathbf{e}}_{\mathbf{k}}, \quad n = 0, \pm 1, \ldots . \tag{5}$$

The continuity of the tangential components of $\mathbf{E}$ and $\mathbf{H}$ at $x=nd+h_2$ and $x=(n+1)d$ can be expressed as a matrix equation $\mathbf{M_E E}=\mathbf{0}$, where $\mathbf{M_E}$ is a 4×4 matrix and the components of $\mathbf{E}$ are the four amplitudes A_j, B_j. This system of equations has nontrivial solutions only if $\det(\mathbf{M_E})=0$. This condition gives the dispersion relation

$$\cos k_B d = \cos K_1 h_1 \cos K_2 h_2 - \frac{1}{2}\left(\frac{K_1}{K_2} + \frac{K_2}{K_1}\right)\sin K_1 h_1 \sin K_2 h_2. \tag{6}$$

In Fig. 2(a) we show the band structure obtained from Eq. (6) for a 1D PC made of high-ϵ layers ($\epsilon_2=16$) separated by air ($\epsilon_1=1$), describing a monolithic Ge SL. In this figure, the frequency and the parallel wave vector have been normalized to the period d of the SL. Propagating Bloch waves are present when the Bloch wave vector k_B is real. On the other hand, imaginary values of k_B give rise to forbidden bands. For sufficiently large values of $k_\parallel$, according to Eq. (4), K_1 becomes imaginary and the electric field has evanescent behavior in the air while it is waveguided in the dielectric. The modes below the light line in air are radiative modes, and the part of the bands above the light line corresponds to evanescent modes.

B. TM normal modes

Because the dielectric function ϵ varies periodically with x, then, for TM polarization, the magnetic induction field is given in the Bloch-wave form

$$\mathbf{B}_{\mathbf{k}}(\mathbf{r}) = u_{k_B}(x)e^{ik_B x}e^{i(k_y y + k_z z)}\hat{\mathbf{e}}_{\mathbf{k}}, \tag{7}$$

where $\hat{\mathbf{e}}_{\mathbf{k}}$ is a unitary vector defined as in Eq. (2). In analogy to Eq. (3), the magnetic induction field in each layer in the unit cell $n=0$ can be written as the combination of two plane waves propagating to the right and left:

$$\mathbf{B}_{\mathbf{k}}^{(0,j)}(x) = [A_j e^{iK_j(x)} + B_j e^{-iK_j(x)}]\hat{\mathbf{e}}_{\mathbf{k}}, \tag{8}$$

where K_j is defined in Eq. (4). Invoking the Bloch theorem, we can obtain the solutions in the nth cell,

$$\mathbf{B}_{\mathbf{k}}^{(n,j)}(x) = e^{ink_B d}[A_j e^{iK_j(x-nd)} + B_j e^{-iK_j(x-nd)}]\hat{\mathbf{e}}_{\mathbf{k}}. \tag{9}$$

The continuity of the tangential components of $\mathbf{E}$ and $\mathbf{H}$ at $x=nd+h_2$ and $x=(n+1)d$ can be expressed as a matrix equation $\mathbf{M_B B}=\mathbf{0}$, where $\mathbf{M_B}$ is a 4×4 matrix and the components of $\mathbf{B}$ are the four amplitudes A_j, B_j. To obtain nontrivial solutions the condition $\det(\mathbf{M_B})=0$ must be fulfilled. This requirement provides the dispersion relation for TM modes,

$$\cos k_B d = \cos K_1 h_1 \cos K_2 h_2 - \frac{1}{2}\left(\frac{K_1\epsilon_2}{K_2\epsilon_1} + \frac{K_2\epsilon_1}{K_1\epsilon_2}\right)\sin K_1 h_1 \sin K_2 h_2. \tag{10}$$

Equations (6) and (10) are in agreement with Ref. [43]. In Fig. 4(a) we present the band structure obtained from the dispersion relation in Eq. (10). The bands touch each other when $k_\parallel = \omega \sin\theta_B / c$, with θ_B as the Brewster angle, where waves with TM polarization propagate without any reflection from layer 1 to layer 2 and vice versa.

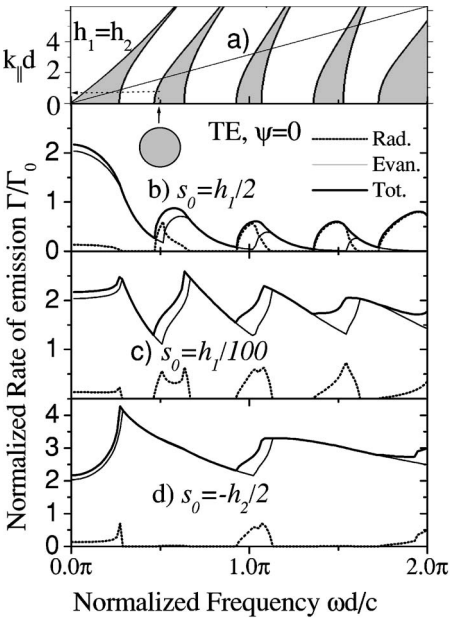

FIG. 2. (a) TE band structure for the PC shown in Fig. 1 with $h_1=h_2=d/2$. Gray areas indicate allowed bands and $k_\parallel d$ is the normalized wave-vector component parallel to the interfaces. (b)–(d) TE contribution to the rate of SE of an atom with dipole moment parallel to the layers. The dipole position is (b) $s_0=h_1/2$ (at the middle of the air layer), (c) $s_0=h_1/100$ (very close to the high-index dielectric layer), and (d) $s_0=-h_2/2$, in the middle of the high-ϵ layer. The rate of emission is normalized to that of the vacuum. The emitted power (thick solid lines) can excite both radiative (dotted lines) and evanescent (thin solid lines) modes. The horizontal arrow in part (a) indicates the maximum value of $k_\parallel d$ of the radiation if the $\omega d/c$ value is given by the vertical arrow in (b). Thus the radiation is restricted to a cone, around the PC axis.

III. MODE NORMALIZATION

In Sec. II it was shown that the condition $\det(\mathbf{M})=0$ must be fulfilled in order to get nontrivial solutions. Thus, we can choose an arbitrary value for one of the field amplitudes A_j, B_j. However, using the normalization condition

$$\int d^3r\epsilon(\mathbf{r})\mathbf{a}^*_{\mathbf{k}'}(\mathbf{r})\cdot\mathbf{a}_{\mathbf{k}}(\mathbf{r})=\delta(\mathbf{k}-\mathbf{k}'), \tag{11}$$

which must be satisfied to ensure that the $\mathbf{a}_{\mathbf{k}}(\mathbf{r})$ form a set of orthonormal functions [4,35], we can assign a definite value to all the amplitudes. Using the Bloch theorem, we can write $\mathbf{a}_{\mathbf{k}}^{(n,j)}$ in terms of the vector potential in the cell $n=0$,

$$\sum_{n=-\infty}^{\infty} e^{in(k_B-k'_B)d}\left[\int_{-\infty}^{\infty}dy\,dz\int_0^{h_2}dx\;\epsilon_2\mathbf{a}_{\mathbf{k}'}^{(0,2)*}\cdot\mathbf{a}_{\mathbf{k}}^{(0,2)}+\int_{-\infty}^{\infty}dy\,dz\int_{h_2}^{d}dx\;\epsilon_1\mathbf{a}_{\mathbf{k}'}^{(0,1)*}\cdot\mathbf{a}_{\mathbf{k}}^{(0,1)}\right]=\delta(\mathbf{k}-\mathbf{k}'). \tag{12}$$

A. TE mode normalization

When we substitute the vector potential in the previous equation, using the Coulomb gauge $\mathbf{E}_{\mathbf{k}}(\mathbf{r})=i(\omega_{\mathbf{k}}/c)\mathbf{a}_{\mathbf{k}}(\mathbf{r})$, the Eq. (5), and after integrating over x we get

$$\epsilon_2\left\{(|A_2|^2+|B_2|^2)h_2+2\,\mathrm{Re}\left[A_2^*B_2\frac{e^{-2iK_2h_2}-1}{-2iK_2}\right]\right\}+\epsilon_1\left\{(|A_1|^2+|B_1|^2)h_1+2\,\mathrm{Re}\left[A_1^*B_1\frac{e^{-2iK_1d}-e^{-2iK_1h_2}}{-2iK_1}\right]\right\}=\frac{\omega_{\mathbf{k}}^2d}{(2\pi)^3c^2}. \tag{13}$$

This equation, together with the matrix equation $\mathbf{M_E}\mathbf{E}=\mathbf{0}$, determines the constants A_1, B_1, A_2, and B_2.

B. TM mode normalization

Because the mode normalization in Eq. (11) must be fulfilled, we need to express the vector potential in terms of the magnetic induction field. Inverting the relation $\mathbf{B}_{\mathbf{k}}(\mathbf{r})=\nabla\times\mathbf{a}_{\mathbf{k}}(\mathbf{r})$,

$$\mathbf{a}_{\mathbf{k}}(\mathbf{r})=\frac{c^2}{\epsilon(\mathbf{r})\omega^2}\nabla\times\mathbf{B}_{\mathbf{k}}(\mathbf{r}). \tag{14}$$

In the 0th cell, substituting Eq. (8) in Eq. (14), we obtain

$$\mathbf{a}_{\mathbf{k}}^{(j)}(\mathbf{r})=e^{i(k_yy+k_zz)}[\hat{\mathbf{x}}a_{\mathbf{k}x}^{(j)}(x)+a_{\mathbf{k}T}^{(j)}(x)(\hat{\mathbf{y}}\sin\phi+\hat{\mathbf{z}}\cos\phi)], \tag{15}$$

with ϕ being the angle between $\mathbf{k}_\parallel$ and the z axis (see Fig. 1) and where we have defined

$$a_{\mathbf{k}x}^{(j)}(x)=\frac{c^2}{\epsilon_j\omega^2}ik_\parallel[A_je^{iK_jx}+B_je^{-iK_jx}], \tag{16}$$

$$a_{\mathbf{k}T}^{(j)}(x)=-\frac{c^2}{\epsilon_j\omega^2}iK_j[A_je^{iK_jx}-B_je^{-iK_jx}], \tag{17}$$

and the superscript (0) which refers to the cell $n=0$ is dropped hereafter.

Substituting Eq. (15) into Eq. (12), we obtain

$$\epsilon_2\int_0^{h_2}dx[|a_{\mathbf{k}x}^{(2)}(x)|^2+|a_{\mathbf{k}T}^{(2)}(x)|^2]+\epsilon_1\int_{h_2}^{d}dx[|a_{\mathbf{k}x}^{(1)}(x)|^2+|a_{\mathbf{k}T}^{(1)}(x)|^2]=\frac{d}{(2\pi)^3}. \tag{18}$$

Substituting Eqs. (16) and (17) into Eq. (18) and integrating we get

$$\frac{1}{\epsilon_1}\left\{\frac{\omega^2}{c^2}\epsilon_1h_1(|A_1|^2+|B_1|^2)+2(k_\parallel^2-K_1^2)\mathrm{Re}\left[A_1B_1^*\frac{e^{-2iK_1h_2}-e^{-2iK_1d}}{2iK_1}\right]\right\}+\frac{1}{\epsilon_2}\left\{\frac{\omega^2}{c^2}\epsilon_2h_2(|A_2|^2+|B_2|^2)+2(k_\parallel^2-K_2^2)\mathrm{Re}\left[A_2B_2^*\frac{1-e^{-2iK_2h_2}}{2iK_2}\right]\right\}=\frac{\omega^4d}{(2\pi)^3c^4}, \tag{19}$$

where Re means "real part of."

Using the matrix equation $\mathbf{M_B}\mathbf{B}=\mathbf{0}$, we can write B_1, A_2, and B_2 in terms of A_1 which is determined by this mode normalization condition.

IV. EMITTED POWER

We assume that the dipole is oscillating with frequency ω_0 at the point $\mathbf{r}_0=(x_0=h_2+s_0,y_0,z_0)$, see Fig. 1, and has a moment $\hat{\boldsymbol{\mu}}=\hat{\mathbf{x}}\sin(\psi)+\hat{\mathbf{y}}\cos(\psi)$ (taken, without limitation of the generality, in the xy plane).

A. TE emitted power

In this subsection we calculate the TE contribution to the emitted power; it is given by Eq. (1) with the subindex p =TE. The vector potential at the emitter's position is

$$\mathbf{a}_{\mathbf{k}}(\mathbf{r_0})=\frac{-ic}{\omega_{\mathbf{k}}}[A_1e^{iK_1(h_2+s_0)}+B_1e^{-iK_1(h_2+s_0)}]e^{i(k_yy_0+k_zz_0)}\hat{\mathbf{e}}_{\mathbf{k}}, \tag{20}$$

with

$$\hat{\mathbf{e}}_{\mathbf{k}}=-\hat{\mathbf{y}}\cos\phi+\hat{\mathbf{z}}\sin\phi, \tag{21}$$

using the fact that $\hat{\mathbf{e}}_{\mathbf{k}}\perp\mathbf{k}_\parallel$ (see inset of Fig. 1). Using these expressions, we get

$$|\mathbf{a}_{\mathbf{k}}(\mathbf{r_0})\cdot\hat{\boldsymbol{\mu}}|^2=\cos^2\phi\cos^2\psi\frac{c^2}{\omega_{\mathbf{k}}^2}[|A_1|^2+|B_1|^2+2\,\mathrm{Re}(A_1^*B_1e^{-2iK_1(h_2+s_0)})]. \tag{22}$$

To calculate the integral in Eq. (1) we employ cylindrical coordinates where $\mathbf{k}=(k_\parallel,\phi,k_B)$, and $d^3k=k_\parallel dk_\parallel d\phi dk_B$. Thus, integrating over ϕ, the TE contribution to Eq. (1) can be written as

$$P_{\mathrm{TE}}=\pi^3c^2\mu^2\cos^2\psi\int dk_\parallel k_\parallel\int dk_B[|A_1|^2+|B_1|^2+2\,\mathrm{Re}(A_1^*B_1e^{-2iK_1(h_2+s_0)})]\delta(\omega_{\mathbf{k}}-\omega_0). \tag{23}$$

For the Dirac-δ function in the integrand, we use the property

$$\delta(f(x)) = \sum_{x_n} \frac{\delta(x - x_n)}{|df/dx_n|}, \tag{24}$$

where x_n are the zeros of the function $f(x)$. For a given $k_\parallel$ there are two values $\pm k_B$ satisfying $\omega_{\mathbf{k}} = \omega_0$; thus the integration over k_B reduces to

$$P_{\mathrm{TE}} = 2\pi^3 c^2 \mu^2 \cos^2\psi \int dk_\parallel k_\parallel \left| \frac{dk_B}{d\omega_0} \right| [|A_1|^2 + |B_1|^2 + 2\,\mathrm{Re}(A_1^* B_1 e^{-2iK_1(h_2+s_0)})]\Big|_{\omega=\omega_0}. \tag{25}$$

The emitted power is given by the last equation and is a function of the frequency ω_0, the dipole position x_0 and orientation ψ, and of the material (ϵ_1 and ϵ_2) and geometrical (h_1 and h_2) parameters of the PC. The integration must be over the allowed modes provided by the dispersion relation in Eq. (6) with real Bloch wave vector k_B. The value of k_B depends on the selected frequency ω_0 and on the integration variable $k_\parallel$, as determined by Eq. (6). Moreover, taking layer 1 as the low-ϵ layer, the modes are radiative if $k_\parallel < \omega\sqrt{\epsilon_1}/c$; otherwise they are evanescent. The contribution of each type of modes can be readily obtained by splitting the integration region over $k_\parallel$. The power emitted by the dipole can give rise to propagating waves if radiative modes are excited. If the dipole emission couples to evanescent modes, then the waves are guided by the high-ϵ layer and decay away from the interfaces in the low-ϵ layer. If the dipole is oriented perpendicular to the interfaces ($\psi = \pi/2$), the dipole coupling to TE polarized modes vanishes, as can be noted from the factor $\cos^2\psi$ outside the integral. The contribution of TM modes to the emitted power is investigated in the next subsection.

B. TM emitted power

The TM contribution to the emitted power is given by the index $p = TM$ in Eq. (1). Using cylindrical coordinates, and the vector potential given in Eqs. (15)–(17), after integrating over ϕ we get

$$P_{\mathrm{TM}} = \frac{2\pi^3 c^4 \mu^2}{\epsilon_1^2 \omega^2} \int dk_\parallel k_\parallel \int dk_B [(|A_1|^2 + |B_1|^2) I(\psi) + 2J(\psi)\mathrm{Re}(A_1^* B_1 e^{-2iK_1(h_2+s_0)})]\delta(\omega_{\mathbf{k}} - \omega_0), \tag{26}$$

where

$$I(\psi) \equiv k_\parallel^2 \sin^2\psi + \frac{1}{2} K_1^2 \cos^2\psi, \tag{27}$$

$$J(\psi) \equiv k_\parallel^2 \sin^2\psi - \frac{1}{2} K_1^2 \cos^2\psi. \tag{28}$$

For the integration over k_B, we retrace the steps used in the TE emitted power; then, the expression for the TM power is given in terms of a single integration over $k_\parallel$:

$$P_{\mathrm{TM}} = \frac{4\pi^3 c^4 \mu^2}{\epsilon_1^2 \omega^2} \int dk_\parallel k_\parallel \left| \frac{dk_B}{d\omega_0} \right| [(|A_1|^2 + |B_1|^2) I(\psi) + 2J(\psi)\mathrm{Re}(A_1^* B_1 e^{-2iK_1(h_2+s_0)})]\Big|_{\omega=\omega_0}. \tag{29}$$

In contrast to the power emitted into TE modes, here the dependence on the dipole orientation is more complicated, and both perpendicular ($\psi = \pi/2$) and parallel ($\psi = 0$) dipoles can radiate into TM modes. In fact, the power emitted into TM-polarized modes by a dipole with arbitrary orientation can be represented as a linear combination of the powers emitted for the two independent orientations $\psi = 0$ and $\psi = \pi/2$:

$$P_{\mathrm{TM}}(\psi) = \cos^2\psi P_{\mathrm{TM}}(\psi = 0) + \sin^2\psi P_{\mathrm{TM}}(\psi = \pi/2). \tag{30}$$

Explicitly,

$$P_{\mathrm{TM}}(\psi = 0) = \frac{2\pi^3 c^4 \mu^2}{\epsilon_1^2 \omega^2} \int dk_\parallel k_\parallel K_1^2 \left| \frac{dk_B}{d\omega_0} \right| [|A_1|^2 + |B_1|^2 - 2\,\mathrm{Re}(A_1^* B_1 e^{-2iK_1(h_2+s_0)})]\Big|_{\omega=\omega_0}, \tag{31}$$

$$P_{\mathrm{TM}}(\psi = \pi/2) = \frac{4\pi^3 c^4 \mu^2}{\epsilon_1^2 \omega^2} \int dk_\parallel k_\parallel^3 \left| \frac{dk_B}{d\omega_0} \right| [|A_1|^2 + |B_1|^2 + 2\,\mathrm{Re}(A_1^* B_1 e^{-2iK_1(h_2+s_0)})]\Big|_{\omega=\omega_0}. \tag{32}$$

Analogously to the previous subsection, the integration is over the pass bands, with both radiative and evanescent contributions, obtained from the TM dispersion relation, Eq. (10). Note that the calculation up to this point is analytic, and the power emitted is given in terms of a single integration.

V. SPECIAL CASES

A. Long-wavelength limit $\omega d/c \to 0$

In this limit, the SL is known to exhibit form birefringence, so its optical properties must be described in terms of ordinary (ϵ_{or}) and extraordinary (ϵ_{ext}) dielectric constants [43]. In the low-frequency region both $k_\parallel$ and k_B are very small in comparison to $1/d$. Thus $K_1, K_2 \ll 1/d$ as can be seen from Eq. (4). With these approximations, the dispersion relation for TE modes reduces to

$$k_B^2 + k_\parallel^2 = \frac{\omega^2}{c^2} \epsilon_{\mathrm{or}}, \tag{33}$$

where $\epsilon_{\mathrm{or}} \equiv \epsilon_1 f_1 + \epsilon_2 f_2$, and $f_1 = h_1/d$, $f_2 = h_2/d$ (the filling fractions of layers 1 and 2, respectively). The equifrequency surfaces are spheres of radius $(\omega/c)\sqrt{\epsilon_{\mathrm{or}}}$, and the integral that gives the TE contribution can be solved analytically. The result for the normalized power is

$$\frac{P_{\mathrm{TE}}}{P_0} \to \frac{3}{4} \cos^2\psi \sqrt{\epsilon_{\mathrm{or}}}. \tag{34}$$

Turning to the TM contribution, the dispersion relation, Eq. (10), in the low-frequency limit is

$$\frac{k_B^2}{\epsilon_{\mathrm{or}}} + \frac{k_\parallel^2}{\epsilon_{\mathrm{ext}}} = \frac{\omega^2}{c^2}. \tag{35}$$

The equifrequency surface is now an ellipsoid of revolution with $1/\epsilon_{\mathrm{ext}} \equiv f_1/\epsilon_1 + f_2/\epsilon_2$. It is convenient to separately calculate the limit of the emitted power for the two independent

dipole orientations $\psi=0$ and $\psi=\pi/2$. When the dipole is parallel to the interface ($\psi=0$) the integral in Eq. (31) is reduced to

$$\frac{P_{\mathrm{TM}}(\psi=0)}{P_0} \to \frac{1}{4}\frac{\epsilon_{\mathrm{ext}}}{\sqrt{\epsilon_{\mathrm{or}}}}. \tag{36}$$

On the other hand, if the dipole is perpendicular to the interfaces ($\psi=\pi/2$), using Eq. (32), the power emitted by a dipole immersed in layer j is

$$\frac{P_{\mathrm{TM}}(\psi=\pi/2)}{P_0} \to \frac{\sqrt{\epsilon_{\mathrm{or}}}\epsilon_{\mathrm{ext}}^2}{\epsilon_j^2}. \tag{37}$$

The case of an emitter embedded in a slab with dielectric constant ϵ_1, bounded by semi-infinite dielectrics ϵ_2 [12], can be obtained by applying the limit $f_2 \gg f_1$. Particularly, in [12] the long-wavelength limit was obtained and it agrees with the limit $f_2 \gg f_1$ applied to Eqs. (34), (36), and (37).

In this long-wavelength limit we expected to obtain results for the emission rates in an arbitrary uniaxial optical medium. This does occur, indeed, for TE polarization and for TM polarization with the dipole parallel to the interfaces. When the dipole is perpendicular to the interfaces, however, the power emitted depends not only on ϵ_{or} and ϵ_{ext} but also on the dielectric constant ϵ_j of the layer hosting the atom. Thus if we first homogenized the PC and then calculated the rate of emission of an atom embedded in this effective uniaxial medium, the result would have differed from Eq. (37), obtained in the long-wavelength limit for the dipole-PC system. In this subsection, we applied the limit $\omega d/c \to 0$ to the entire system which does not homogenize in the TM ($\psi=\pi/2$) configuration because the perpendicular component of the electric field E_x is discontinuous across the interface between the two media in the unit cell which contains the radiator. For parallel dipoles, this normal component of the electric field does not contribute to the emitted power due to the dot product in Eq. (1).

B. Comparison with the "Dirac comb" model

The "Dirac comb" model of the SL [32,33] corresponds to a limiting case of the ordinary SL: very narrow layers ($h_2 \to 0$) with very large dielectric constant ($\epsilon_2 \to \infty$) separated by low-index layers with the ratio $\epsilon_2 h_2/d$ being a finite number (g). The dispersion relation for the TE modes of a Dirac comb SL was derived in Ref. [44] and gives rise to a TE band structure that is qualitatively similar to that obtained from a realistic modelling of the SL. For the TM modes, the Dirac comb model has the drawback that neither the Brewster effect nor the evanescent modes occur in its band structure [45]. Thus the Dirac comb model fails when calculating the TM contribution to the emitted power.

In Ref. [32], an expression for the emitted power into the TE modes of a Dirac comb SL was computed. In fact, the analytic expression for the emitted power given in Ref. [32] is recovered by applying the limits required by the Dirac comb model to the Eq. (25). In particular, the agreement is apparent from the limit $\omega d/c \to 0$; Eq. (34) reduces to $P_{\mathrm{TE}}/P_0 \to (3/4)\sqrt{1+g}\cos^2\psi$ which is the same result obtained in Ref. [32]. Taking the limit $\epsilon_2 h_2/d \to g$ in Eqs. (31) and (32) we obtain, respectively, the expressions for the power emitted by a dipole with orientations $\psi=0$ and $\psi=\pi/2$ given in Ref. [33].

VI. RESULTS AND DISCUSSION

In all the figures to be displayed the configuration is given by Fig. 1 with $\epsilon_1=1$ and $\epsilon_2=16$ (for Ge).

A. Rate of emission spectra—TE polarization

In Fig. 2 we show the band structure and SE spectra for TE polarization and three positions of the dipole within a unit cell. The air and dielectric layers have equal widths. It should be noted that the allowed bands in Fig. 2(a), shown in gray and calculated from Eq. (6), are either radiative or evanescent depending on their location relative to the light line in air $k_\parallel=\omega/c$. The radiative modes ($k_\parallel<\omega/c$) are located below the light line. The evanescent modes ($k_\parallel>\omega/c$), located above the light line, decay in the air and are waveguided by the high-index layers. Although there are frequency regions where *radiative* modes are absent, the allowed bands move toward higher frequencies (and become narrower) when the parallel component of the wave vector is increased. Therefore, for any frequency value, we can always find available modes. Because the dipole emission can couple to both radiative and evanescent modes, the SE rate will not vanish for any frequency. The coordinate $\omega d/c$ can be interpreted as either the frequency of the emitted photon scaled with the period d or as the period of the PC normalized to the frequency of the emitted photon. The first point of view is widely used in the PC literature, but the second approach is convenient when studying decay rates because the emission frequency is determined by differences in fixed energy levels.

The rate of emission for an emitter located at the middle of the air layer is shown in Fig. 2(b). Here, the rate of emission presents an oscillatory behavior which, as we will show, is related to the photonic band structure. In the spectral range $0.27\pi \lesssim \omega d/c \lesssim 0.48\pi$ there is no radiative emission as a result of the absence of radiative modes; this is associated with *internal* omnidirectional reflection. The same occurs for higher frequencies, namely for $0.67\pi \lesssim \omega d/c \lesssim 0.92\pi$, $1.12\pi \lesssim \omega d/c \lesssim 1.37\pi$, etc. In these frequency ranges the radiated light is then TM polarized. For frequencies around the band edges for on-axis propagation the density of modes is very high as a result of the low group velocity. Thus one could expect an important enhancement in the radiative contribution to the rate of SE at the band edges $\omega d/c = 0.27\pi$, 0.48π, etc. However, while there is an abrupt increase in the rate of SE at the lower band edges ($\omega d/c = 0.48\pi$, 0.92π, etc.), this does not occur at the upper band edges ($\omega d/c = 0.27\pi$, 1.12π,...). Thus the rate of SE is not necessarily proportional to the density of modes. From Eq. (1) the SE depends on the interaction term $|\mathbf{a}_{\mathbf{k}p}(\mathbf{r_0})\cdot\hat{\boldsymbol{\mu}}|$. Thus in order to explain the behavior of the rate of emission, the value of the electric field [Eq. (5)] at the position of the emitter must also be taken into account. These normal modes

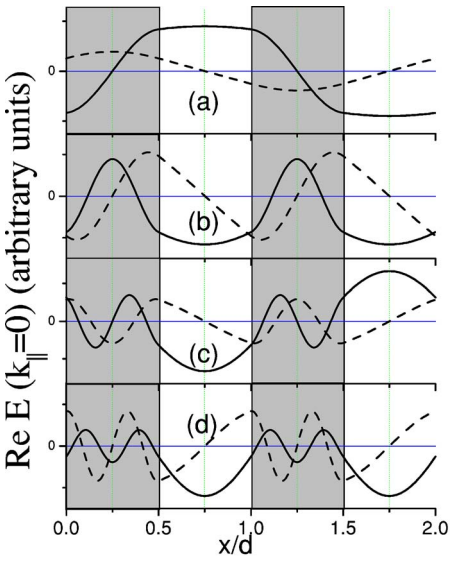

FIG. 3. (Color online) Electric field modes at the edges of the band gaps for $k_\parallel=0$. The dashed and solid lines correspond to lower and upper edges respectively for (a) the first, (b) second, (c) third, and (d) fourth band gaps.

at the band edges with $k_\parallel=0$ are shown in Fig. 3. At the upper band edges (dashed lines), the electric field presents a node at the middle of the air layer. Therefore the interaction term and, consequently, the SE in the direction perpendicular to the interfaces vanishes at the upper band edges despite the high density of available states. On the other hand, the antinodes of the modes at the lower band edges at the emitter's position lead to the fast increase of the radiative emission rate, which is also manifested as slope discontinuities in the total TE-polarized SE. This enhancement of emission was pointed out by Dowling [36] who calculated the emission by a dipole in a finite PC although limiting the analysis to the scalar approximation with $k_\parallel=0$. At $\omega d/c$ values where the lower band edges cross the light line ($\omega d/c=0.52\pi$, 1.05π, etc.), an increase in the SE into the now available evanescent modes can be noted. However, at the same frequency values, the radiative component decreases sharply, which results in a cancellation of the radiative and evanescent "kinks" as can be seen in the smooth total TE-polarized emission.

Some features of the (directional) radiation pattern can be extracted from the band structure. For instance, at frequencies corresponding to the radiative maxima in Fig. 2(b) ($\omega d/c=0.52\pi$, 1.05π, etc.), the radiation occurs in all directions in space because there is no limitation in the permitted values of $k_\parallel$ ($0\leqslant k_\parallel<\omega/c$); however, as ω or d decreases and approaches the band edge for on-axis propagation ($\omega d/c \rightarrow 0.48\pi$, 0.92π, etc.), $k_\parallel$ becomes limited to values below a certain $k_{\max}(\omega)$. For example, if $\omega d/c$ is given by the vertical arrow [Fig. 2(b)] the maximal value of $k_\parallel d$ is given by the horizontal arrow, and this value is smaller than $(\omega/c)d$. This means that the radiation is restricted to a cone, around the PC axis, of angle $\sin^{-1}[k_{\max}(\omega)c/\omega]$. For $\omega d/c \geqq \pi$ (or $d \geqq \lambda/2$) the maxima in the total TE-polarized emission are mostly due to radiative SE. In other words, evanescent modes are dominant only when the distance from the emitter to an interface, which in Fig. 2(b) is $s_0=d/4$, is shorter than about $\lambda/8$. For larger separations, the evanescent contribution becomes very small; this effect can be used in combination with the absence of radiative emission in the *internal* omnidirectional gaps to achieve strong inhibition of TE-polarized SE, see Fig. 2(b) at $\omega \simeq 1.35\pi$.

For other dipole positions in the air layer, the modes do not present a node; as a result, discontinuities at both the upper and the lower edges for $k_\parallel=0$ should appear. It is in fact the case shown in Fig. 2(c) where the emitter is located very close to a high-ϵ layer. In the frequency range displayed, the evanescent contribution to the rate of emission dominates. It can be explained by the fact that the high-index layer is in the near field of the dipole.

We also calculated the rate of emission when the emitter is located inside the high-ϵ material. In Fig. 2(d) the rate of emission by an atom at the midpoint of the dielectric layer is plotted. The rate of emission here also follows the on-axis band structure. However, contrary to the case of an atom at the middle of the air layer, the slope discontinuities do not follow an apparent pattern. Analyzing the field modes at the center of the dielectric layer, Fig. 3, at the middle of the gray areas, the mode at the upper edge of the first band has an antinode at the emitter position which gives rise to a peak in the frequency-dependent rate of emission at $\omega d/c \simeq 0.27\pi$. On the other hand, the total TE-polarized SE in Fig. 2(d) does not present slope discontinuities at the frequencies corresponding to a node, namely at the band edges of the second and fourth bands ($\omega d/c \simeq 0.48\pi$, 0.67π, 1.37π, and 1.55π). It must be noted that at $\omega d/c \simeq 0.27\pi$ (at the peak of the radiative component), which corresponds to the upper band edge of the first band, the contribution of the radiative modes to the total TE-polarized SE is about 20%. Compared to the amount of light that can be extracted from a source in a single layer with $\epsilon=16$ (which is approximately $1/4\epsilon \simeq 1.6\%$ [46,47]), the radiative emission in the 1D PC is 12 times higher.

The low-frequency limit [Eq. (34)] is independent of the dipole position because in this regime the wave does not sense the periodic structure. In fact, Eq. (34) correctly predicts the value $\Gamma/\Gamma_0|_{\omega=0}=2.19$ found in Figs. 2(b)–2(d).

B. Rate of emission spectra—TM polarization

The band structure and the frequency-dependent rate of SE for TM polarization are displayed in Fig. 4. The dipole is oriented parallel to the interfaces ($\psi=0$), and, as in Fig. 2, three dipole positions are considered. The band structure for the TM modes is shown in Fig. 4(a) and the values used in its calculation are the same as in Fig. 2. The main difference between this figure and the band structure for the TE modes is the shrinking in the band gaps for TM modes in the vicinity of the Brewster light line $k_\parallel=\omega \sin\theta_B/c$. Since the dielectric contrast is high, the Brewster line $\omega/c=k_\parallel/\sin\theta_B$ is very close to the light line in air $\omega/c=k_\parallel$ (we note that $\theta_B=\arctan\sqrt{\epsilon_2/\epsilon_1}=\arctan 4 \simeq 76°$, so $\sin\theta_B \simeq 0.97$).

The frequency-dependent rate of emission into TM modes when the emitter is at the midpoint of the air layer and $\psi=0$ is shown in Fig. 4(b). In contrast to the corresponding TE case, here the radiative contribution never vanishes; how-

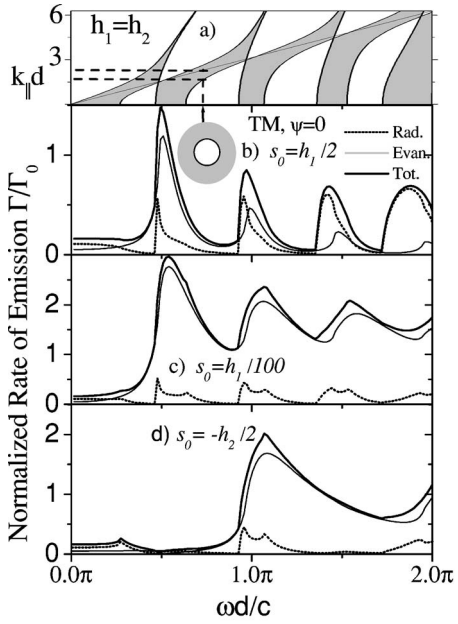

FIG. 4. (a) TM band structure for $h_1=h_2=d/2$. (b)–(d) TM contribution to the SE rate of an atom oriented parallel to the interfaces and located (b) midway between adjacent high-ϵ layers, (c) very near to a layer at $s_0=h_1/100$, and (d) $s_0=-h_2/2$, at the middle of a high-ϵ layer. When $\omega d/c\approx 0.75\pi$, the minimum value of $k_\parallel d$ is given by the lower horizontal dashed line in part (a). This limits the radiation to angles greater than a minimum angle as shown in the illustration in (b).

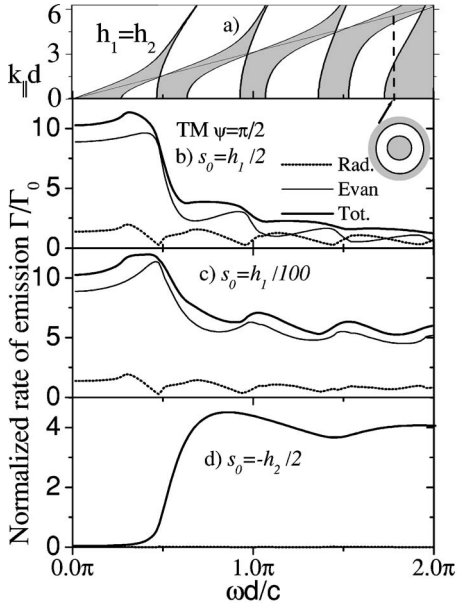

FIG. 5. As in Fig. 4, but with the dipole moment orientated perpendicular to the interfaces ($\psi=\pi/2$). The directional radiation pattern presents a ring of forbidden angles when $\omega d/c$ is given by the arrow in part (b).

ever, its contribution is very small at frequencies just below the lower band edges for on-axis propagation ($\omega d/c \simeq 0.48\pi$, 0.92π, etc.). Hence if the coupling to waveguided modes is also low, which occurs when $\omega d/c>1$ or $s_0>\lambda/8$, then the TM-polarized rate of emission can be very small. What is more, because the on-axis band structure is the same for TE and TM polarization, the total (TE+TM) rate of emission can be strongly inhibited: $\Gamma(\omega=1.35\pi)=0.092\Gamma_0$, from Figs. 2(b) and 4(b). When the dipole is at the middle of the air layer [Fig. 4(b)], the radiative contribution increases sharply at the lower band edges for on-axis propagation. On the contrary, at the on-axis upper band edges the radiative contribution does not present any abrupt change. Due to the nodes of the modes corresponding to the on-axis upper band edges (the same as for TE polarization, Fig. 3) at the dipole position, the emitted power in the direction of the SL axis vanishes. This is associated with the rapid decrease of the peaks in Fig. 4(b). Although less pronounced than for TE-polarized emission, the steep increase in the radiative contribution at the lower band edges for $k_\parallel=0$ (related to the antinodes in Fig. 3) also gives rise to slope discontinuities in the total TM-polarized SE.

The spectra of SE for the dipole positions $s_0=h_1/100$ and $s_0=-h_2/2$ are shown, respectively, in panels (c) and (d) of Fig. 4. Here, the radiative contribution never vanishes but presents peaks at some on-axis band edges similar to the corresponding TE-polarized radiative contribution. When the dipole is at the middle of the dielectric and $\omega d/c<0.4\pi$, the radiative contribution is larger than the evanescent one. However, for larger $\omega d/c$ values, the SE into evanescent modes dominates. In the long-wavelength limit, that is when $\omega d/c\to 0$, the computed value shown in Figs. 4(b)–4(d) is independent of the dipole's position and agrees with that obtained from Eq. (36): $\Gamma_{TM}(\psi=0)\to 0.16\Gamma_0$.

If the dipole is parallel to the interfaces ($\psi=0$), then the TE and the TM contributions to the SE share common features. The spectra of SE for the other basic dipole orientation ($\psi=\pi/2$) are presented in Fig. 5. Here, the band structure and the SE spectra for three dipole positions are displayed. Comparing Figs. 4 and 5, qualitative differences can be observed in the frequency-dependent rate of emission for dipoles parallel ($\psi=0$) and perpendicular ($\psi=\pi/2$) to the interfaces. For $\psi=\pi/2$, the emission spectrum is smoother than the spectrum for a dipole parallel to the interfaces where the coupling to the the electric field modes gives rise to slope discontinuities in the rate of emission at the on-axis band edges. However, when $\psi=\pi/2$, the emission cannot couple to the field modes for on-axis propagation. The on-axis band structure effects are therefore less pronounced for this dipole orientation.

For emitters in the air layer [Figs. 5(b) and 5(c)], the rate of emission for $\omega\lesssim c/d$ is about ten times higher than the free space value. Inserting the parameter values used in this figure into the long-wavelength limit in Eq. (37), we obtain $\Gamma/\Gamma_0=10.3$—in agreement with the computed result. We can also notice that the rate of emission in this quasistatic regime is predominantly into nonradiative modes (waveguided in the dielectric and evanescent in air). While, according to Eq. (37), the strong dielectric contrast is an important factor in the enhancement, the filling fraction plays a major role. If the emitter is in the air layer of a 1D PC with a high filling fraction of the dielectric material, the acceleration of the SE can be very high; for instance, with $f_2=5/6$ we obtain $\Gamma(\omega=0,\ \psi=\pi/2)\simeq 77\Gamma_0$. Although most of this emission is

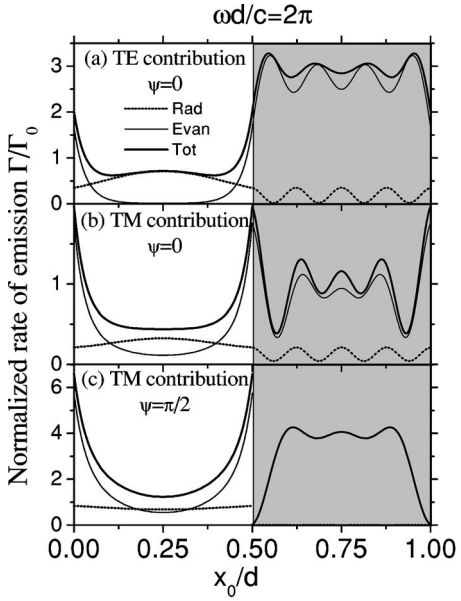

FIG. 6. Rate of emission as a function of the dipole position for a PC with period $d=\lambda$ and $h_1=h_2=d/2$. The white (shaded) regions correspond to a radiator in the air (dielectric). Panels (a), (b), and (c) show the three fundamental configurations.

coupled to guided waves, their conversion to radiation is feasible, as has been experimentally demonstrated for a layered system [48].

From Fig. 4(a) we can see that, at $\omega d/c=0.75\pi$, the radiative emission has a parallel component of the wave vector greater than $k_{\min}\approx 1.7$. Thus the direction of radiation is limited to angles $\alpha>46°$. As discussed for the TE directional radiation pattern, for some values of $\omega d/c$ it is possible to constrain the radiation to a cone. Here, on the contrary, the radiation is prohibited within a cone (defined by the angle $\alpha=46°$). More complicated radiational patterns are also possible. For example, in Fig. 5, for $\omega d/c\simeq 1.8\pi$, there is an annular "hole" in the radiation; that is, there is no radiation for angles α between some $\alpha_{\min}$ and $\alpha_{\max}$.

C. Position-dependent rate of emission

In Fig. 6 we present the rate of SE as a function of the dipole's position for $\omega d/c=2\pi(\lambda=d)$. When the dipole is in air, the evanescent contribution is, as expected, stronger when the dipole is close to a dielectric layer, but it is relatively small when the emitter is at the midpoint between the high-ϵ layers. For both polarizations, the decay rate is continuous across the interfaces when $\psi=0$ [panels (a) and (b)]. On the other hand, when the dipole is perpendicular to the interfaces [TM polarization, panel (c)], the rate of emission satisfies the "boundary condition" $P_1=(\epsilon_2/\epsilon_1)^2P_2$ [17]; it is a signature of the discontinuity of the perpendicular component of the electric field. Consequently, the rate of emission for an emitter just outside the dielectric layer is $(\epsilon_2/\epsilon_1)^2=256$ times greater than for the same emitter just inside the dielectric. This sensitivity could be useful in determining the position of absorbed or adsorbed atoms; however, at separations smaller than a few atomic layers from the interface, the local field effects should be taken into account. In medium 2 (shown in gray) the rate of emission oscillates around the corresponding value in the homogeneous medium. When the high-ϵ layers are enough apart from each other, and the wavelength is of the same order as h_2, the interaction between adjacent dielectric layers is weak. If the dipole is inside a dielectric layer, it will not perceive the other high-ϵ layers, and only the nearest dielectric layer will affect the SE rate of a dipole in air. This situation resembles that of an excited atom in the presence of a single dielectric slab. This system has been widely studied both classically and quantum electrodynamically and, although not shown here, we have reproduced the results given in Ref. [11].

D. Gas of atoms

Finally, we have calculated the rate of emission for a gas of noninteracting emitters in the air layer. In this case, we average the dipole moments over all the directions in space. Thus the factor $\cos^2\psi$ in Eqs. (25) and (29) is replaced by its volume average 1/3, and the factor $\sin^2\psi$ in Eq. (29) has the spatial average of 2/3. We also need to average over the dipole positions s_0. Thus the TE contribution to the radiated power per dipole is

$$P_{\mathrm{TE}}=\frac{2}{3}\pi^3c^2\mu^2\int dk_\parallel k_\parallel\left|\frac{dk_B}{d\omega_0}\right|\left[|A_1|^2+|B_1|^2+2\,\mathrm{Re}\left(A_1^*B_1\frac{e^{-2iK_1d}-e^{-2iK_1h_2}}{-2iK_1h_1}\right)\right]\Bigg|_{\omega=\omega_0}, \tag{38}$$

and, with $I\equiv\frac{2}{3}k_\parallel^2+\frac{1}{6}K_1^2$ and $J\equiv\frac{2}{3}k_\parallel^2-\frac{1}{6}K_1^2$, the TM contribution is

$$P_{\mathrm{TM}}=\frac{4\pi^3c^4\mu^2}{\epsilon_1^2\omega^2}\int dk_\parallel k_\parallel\left|\frac{dk_B}{d\omega_0}\right|\left[(|A_1|^2+|B_1|^2)I+2J\,\mathrm{Re}\left(A_1^*B_1\frac{e^{-2iK_1d}-e^{-2iK_1h_2}}{-2iK_1h_1}\right)\right]\Bigg|_{\omega=\omega_0}. \tag{39}$$

In Fig. 7 the rate of emission per emitter is plotted. The total TE-polarized emission presents slope discontinuities at the band edges for on-axis propagation. Wide frequency regions where the radiative emission is prohibited can also be noted in Fig. 7(a). Although in Fig. 7(b) there exist slope discontinuities, the emission spectrum for the TM power is much smoother than for TE polarization. The TM-polarized rate of emission in the low-frequency regimen is strongly enhanced when compared to the corresponding free-space value. In fact, for narrow air layers ($f_1=1/6$) the rate of emission per atom is 50 times larger than the free space value even for the gas of randomly oriented atoms.

VII. CONCLUSIONS

In this paper we have theoretically investigated the rate of SE of an atom embedded in a perfect 1D PC. Both radiative and evanescent modes were taken into account. Many interesting features in the rate of emission arise from this relatively simple system. The absence of radiative TE-polarized

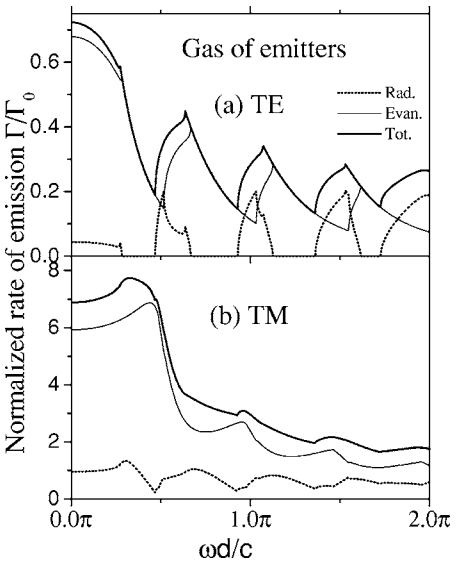

FIG. 7. (a) TE and (b) TM contributions to the rate of emission per emitter for a gas of emitters that are randomly oriented and located in an air layer. Here, $h_1=h_2=d/2$.

emission due to *internal* omnidirectional reflection is a remarkable effect that results in the radiated light being TM polarized. Moreover, strong inhibition of the total rate of emission can be achieved for dipoles that are parallel to the interfaces, in air, oscillating at a frequency somewhat smaller than an upper band-gap edge and provided that the distance s_0 between the emitter and the dielectric is larger than $\lambda/8$. Not only is diminished SE present in a 1D PC, but also an important enhancement has been found, especially for dipoles oriented perpendicularly to the interfaces in the long-wavelength regimen (where analytic results have been derived). This enhancement persists for a gas of atoms in the air layer of a PC with a high filling fraction of dielectric. Although most of this emission goes into waveguide modes, their energy can be extracted by means of a coupling device. Sharp maxima in the radiative emission occur at frequencies corresponding to band edges for on-axis propagation (where the density of states is very high) provided that the emitter is located at an antinode of the electric field. When the atom is embedded in a high-ϵ dielectric layer, the aforementioned maxima in the radiative emission can reach 20% of the total SE which is much higher than the amount of light that can be extracted from a source embedded in a single high-ϵ layer. Some features of the radiation pattern, such as allowed and forbidden annular ranges, can also be deduced from the band structure. Both enhancement and inhibition of the SE should also be observable in a finite PC if the emitter is in the inner cells of a high-contrast PC.

The position of the atom in the unit cell affects the rate of emission considerably. In fact, very rapid variation of the decay rate at the interfaces occurs for dipoles that are perpendicular to the interfaces. This high sensitivity on the position could have important applications in determining the positions of absorbed or adsorbed atoms through the measurement of their rates of SE. Not only the enhancement of SE could be exploited in the improved design of light-emitting devices but also the inhibition of SE could be a desirable characteristic. Thus the 1D PC is an interesting system for experimental investigations. An emitter embedded in a high-contrast 2D PC should also excite coupled waveguide modes that propagate along high-ϵ cylinders. If the filling fraction of the dielectric cylinders is high and the emitter is located in the low-ϵ material, then an enhancement similar to that found in 1D PCs should occur.

ACKNOWLEDGMENTS

This work has been supported by CONACyT Grant No. 41195-F. Also, A.S.S. was financially supported by CONACyT.

[1] E. M. Purcell, Phys. Rev. **69**, 681 (1946).
[2] N. Danz, R. Waldhausl, A. Brauer, and R. Kowarschik, J. Opt. Soc. Am. B **19**, 412 (2002).
[3] E. A. Hinds, in *Cavity Quantum Electrodynamics*, edited by P. R. Berman (Academic Press Inc., Boston, 1994).
[4] R. J. Glauber and M. Lewenstein, Phys. Rev. A **43**, 467 (1991).
[5] K. H. Drexhage, in *Progress in Optics*, edited by E. Wolf (North-Holland, Amsterdam, 1974), Vol. 12.
[6] H. Morawitz and M. R. Philpott, Phys. Rev. B **10**, 4863 (1974).
[7] J. M. Wylie and J. E. Sipe, Phys. Rev. A **30**, 1185 (1984).
[8] W. L. Barnes, J. Mod. Opt. **45**, 661 (1998).
[9] E. Snoeks, A. Lagendijk, and A. Polman, Phys. Rev. Lett. **74**, 2459 (1995).
[10] N. Danz, J. Heber, A. Brauer, and R. Kowarschik, Phys. Rev. A **66**, 063809 (2002).
[11] W. Zakowicz and A. Bledowski, Phys. Rev. A **52**, 1640 (1995).
[12] H. Nha and W. Jhe, Phys. Rev. A **54**, 3505 (1996).
[13] H. P. Urbach and G. L. J. A. Rikken, Phys. Rev. A **57**, 3913 (1998).
[14] S. R. J. Brueck, IEEE J. Sel. Top. Quantum Electron. **6**, 899 (2000).
[15] W. Lukosz and R. E. Kunz, J. Opt. Soc. Am. **67**, 1607 (1977).
[16] W. Lukosz and R. E. Kunz, J. Opt. Soc. Am. **67**, 1615 (1977).
[17] W. Lukosz, Phys. Rev. B **22**, 3030 (1980).
[18] W. Lukosz, J. Opt. Soc. Am. **71**, 744 (1981).
[19] L. Polerecky, J. Hamrle, and B. D. MacCraith, Appl. Opt. **39**, 3968 (2000).
[20] K. G. Sullivan and D. G. Hall, J. Opt. Soc. Am. B **14**, 1160 (1997).
[21] L. Novotny, J. Opt. Soc. Am. A **14**, 91 (1997).
[22] D. Delbeke, R. Bockstaele, P. Bienstman, R. Baets, and H. Benisty, IEEE J. Sel. Top. Quantum Electron. **8**, 189 (2002).
[23] G. Bjork and Y. Yamamoto, IEEE J. Quantum Electron. **27**, 2386 (1991).
[24] I. Alvarado-Rodriguez, P. Halevi, and J. J. Sanchez-

Mondragon, Rev. Mex. Fis. **44**, 268 (1998).
[25] S. M. Dutra and P. L. Knight, Phys. Rev. A **53**, 3587 (1996).
[26] J.-K. Hwang, H.-Y. Ryu, and Y.-H. Lee, Phys. Rev. B **60**, 4688 (1999).
[27] Y. Xu, J. S. Vuckovic, R. K. Lee, O. J. Painter, A. Scherer, and A. Yariv, J. Opt. Soc. Am. B **16**, 465 (1999).
[28] J. D. Joannopoulos, R. D. Meade, and J. N. Winn, *Photonic Crystals—Molding the Flow of Light* (Princeton University Press, Princeton, NJ, 1995).
[29] S. Bastonero, G. P. Bava, G. C. Piat, P. Debernardi, R. Orta, and R. Tascone, Opt. Quantum Electron. **31**, 857 (1999).
[30] P. Yu, P. Bhattacharya, and J.-C. Cheng, J. Appl. Phys. **93**, 6173 (2003).
[31] L. Zhou and G. Li, Opt. Commun. **230**, 347 (2004).
[32] I. Alvarado-Rodriguez, P. Halevi, and A. S. Sanchez, Phys. Rev. E **63**, 056613 (2001); **65**, 039901(E) (2002).
[33] J. R. Zurita-Sánchez, A. S. Sanchez, and P. Halevi, Phys. Rev. E **66**, 046613 (2002).
[34] M. Wubs, L. G. Suttorp, and A. Lagendijk, Phys. Rev. E **69**, 016616 (2004).
[35] J. P. Dowling and C. M. Bowden, Phys. Rev. A **46**, 612 (1992).
[36] J. P. Dowling, J. Lightwave Technol. **17**, 2142 (1999).
[37] A. A. Asatryan, S. Fabre, K. Bush, R. C. McPhedran, L. C. Botten, C. M. de Sterke, and N.-A. P. Nicorovici, Opt. Express **8**, 191 (2001).
[38] S. y Xie, Y. p. Yang, and X. Wu, Eur. Phys. J. D **13**, 129 (2001).
[39] Z.-Y. Li, L.-L. Lin, and Z.-Q. Zhang, Phys. Rev. Lett. **84**, 4341 (2000).
[40] T. Suzuki and P. K. L. Yu, J. Opt. Soc. Am. B **12**, 570 (1995).
[41] J. M. Bendickson, J. P. Dowling, and M. Scalora, Phys. Rev. E **53**, 4107 (1996).
[42] C. Hooijer, D. Lenstra, and A. Lagendijk, Opt. Lett. **25**, 1666 (2000).
[43] P. Yeh, *Optical Waves in Layered Media* (Wiley, New York, 1988).
[44] I. Alvarado-Rodriguez, P. Halevi, and J. Sánchez-Mondragón, Phys. Rev. E **59**, 3624 (1999).
[45] J. R. Zurita-Sánchez and P. Halevi, Phys. Rev. E **61**, 5802 (2000).
[46] I. Schnitzer, E. Yablonovitch, C. Caneau, T. J. Gmitter, and A. Scherer, Appl. Phys. Lett. **63**, 2174 (1993).
[47] M. Rattier, H. Benisty, R. P. Stanley, J.-F. Carlin, R. Houdre, U. Oesterle, C. J. M. Smith, C. Weisbuch, and T. F. Krauss, IEEE J. Sel. Top. Quantum Electron. **8**, 238 (2002).
[48] H. Rigneault, S. Robert, C. Begon, B. Jacquier, and P. Moretti, Phys. Rev. A **55**, 1497 (1997).